ACS OMEGA

Open Access

http://pubs.acs.org/journal/acsodf

Article

Prediction of Hydrogen Diffusion Behavior under the Influence of Defect Structures in Stainless Steel Passivation Film Based on Molecular Dynamics

Yuanshuang Liu,* Feng Qiu,* Mindong Chen, Dingrong Qu, and Haijun Hu

Cite This: *ACS Omega* 2024, 9, 46270−46275

Read Online

ACCESS | Metrics & More | Article Recommendations

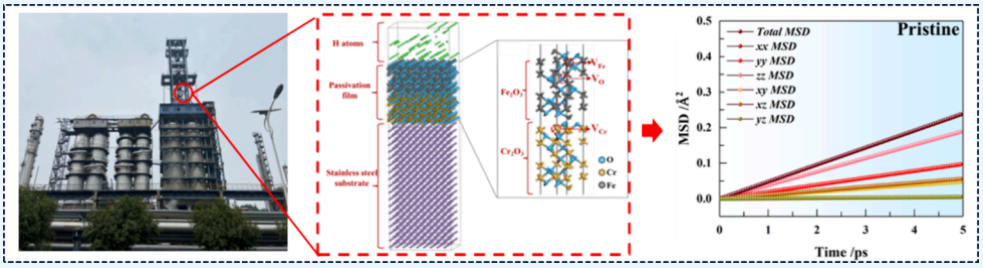

ABSTRACT: The excellent corrosion resistance of stainless steel primarily relies on the formation of a dense passivation film on its surface. Stress corrosion and hydrogen embrittlement are the primary forms of damage to the stainless steel passivation film, leading to film rupture and subsequent corrosion of the stainless steel substrate. The passivation film exhibits semiconducting properties and typically consists of a bilayer structure with a chromium-rich inner layer and an iron-rich outer layer. This study employs molecular dynamics simulations to investigate the interaction energy between hydrogen atoms and pristine stainless steel passivation films (Fe_2O_3/Cr_2O_3) as well as those containing three different types of defects and predicts the diffusion processes of hydrogen atoms in passivation films. The results indicate that the strongest interaction energy of −1.4402 eV is observed between hydrogen atoms and the pristine passivation film. However, as defects emerge within the passivation film, the interaction energy decreases, with a minimum energy of −0.1931 eV observed for the film containing chromium vacancies (V_{Cr}), representing a nearly one-order-of-magnitude reduction compared to the defect-free case. Furthermore, the diffusion coefficients of hydrogen atoms in the three defective passivation films are calculated as 6.437×10^{-10}, 8.249×10^{-10}, and 50.892×10^{-10} m^2/s, respectively. Notably, the presence of a V_{Cr} defect enhances the hydrogen diffusion coefficient by an order of magnitude compared to the pristine film. Anisotropic diffusion paths and properties are elucidated through an analysis of the self-diffusion behavior of hydrogen in different detective passivation films, providing a theoretical basis for the prediction of hydrogen-induced cracking and the development of early warning technologies for passivation film surface failure.

1. INTRODUCTION

The excellent corrosion resistance of stainless steel primarily stems from the formation of a dense passivation film on its surface. Stress corrosion and hydrogen embrittlement are the primary forms of damage to this passivation film, leading to film rupture and subsequent corrosion of the stainless-steel substrate. Hydrogen embrittlement plays a major role in the degradation of the passivation films. Hydrogen, water, hydrogen sulfide, and other hydrogen-containing gases can easily dissociate on the surface of stainless steel, producing hydrogen atoms adsorbed on the surface of stainless steel and further diffusing into the interior of the steel. Then, hydrogen atoms diffuse through the film's defect structures, interact with these defects, and cause them to propagate and evolve. This leads to irreversible hydrogen-induced cracking, which is a manifestation of hydrogen embrittlement and causes the passivation film to rupture, exposing the base material to corrosive media directly.[1,2] Hydrogen also modifies the composition, semiconducting properties, and corrosion resistance of the passivation film.[3−5] Research indicates that the passivation film consists of a bilayer oxide structure with a chromium-rich inner layer and an iron-rich outer layer,[5−7] and its hydrogen barrier capability is closely related to its composition and structure.[8−10] Previous studies have[11] investigated hydrogen bubbling behavior at the interface between aluminum metal and its oxide, revealing that a small

Received: August 4, 2024
Revised: October 20, 2024
Accepted: October 24, 2024
Published: November 11, 2024

number of hydrogen atoms can induce Wulff reconstruction at the interface, resulting in the creation of pores. As the number of hydrogen atoms increases, the pores reach a critical size, accompanied by an increase in the internal pressure, leading to bubbling and film rupture. The preferential accumulation of hydrogen atoms at the interfaces is primarily attributed to the defects present there. According to the point defect model, point defects are easily generated and annihilated at the substrate−film interface, film−solution interface, and within the passivation film.[12,13] The presence of hydrogen degrades the corrosion resistance of stainless steel, enhancing its sensitivity to pitting corrosion. Hydrogen reduces the breakdown potential of the passivation film, thereby degrading its corrosion resistance[14] and promoting the initiation and progression of pitting corrosion. Experimentally, it was found that pristine Cr_2O_3 in the passivate film before electrochemical hydrogen charging prevents pitting corrosion from occurring, thus reducing pitting corrosion sensitivity. However, after electrochemical hydrogen charging, hydrogen increases the defects and disorder in the passivation film, which promotes the growth rate of pitting, resulting in higher pitting corrosion sensitivity.[15,16] Another new explanation for the reduction of corrosion resistance of passivated membranes by hydrogen has been proposed, which suggests that hydrogen introduces an additional electrostatic repulsion between Fe^{2+} or Fe^{3+} and oxygen vacancies that enhances the transport of cationic and anionic vacancies in the intramembrane interstitial space, leading to an increase in the concentration of ferrous ions and oxygen vacancies, which results in a degradation of the structure of the membrane.[17] Consequently, the intrusion of hydrogen atoms into the metal passivation film not only alters its semiconducting properties but also degrades its corrosion resistance, further increasing the possibility of film rupture.[18,19]

Defect diffusion barriers are impacted by point defects, which are sources of defects that attract or annihilate defects and are more common at passivation film interfaces, where the number of chemical bonds between atoms is mismatched. Furthermore, the increase of defects at the passivation film further impacts corrosion resistance. While numerous experimental studies have analyzed the growth theories, semiconducting properties, and corrosion resistance of stainless steel passivation films,[9,20] microscopic investigations of the film remain scarce. In addition, the diverse types of defects encountered in experimental studies make it challenging to discern which point defects promote hydrogen damage and which inhibit it. Therefore, exploring the electrical properties of passivation films at the atomic and electronic scales is crucial for understanding the mechanisms of stress corrosion and hydrogen embrittlement in stainless steel. Uncovering the fundamental interactions between passivation film defect structures and hydrogen atoms will facilitate the fundamental improvement and enhancement of the film's hydrogen resistance, which is of great significance for the development of corrosion protection technologies and ensuring the safe operation of petrochemical equipment.

2. MATERIALS AND METHODS

To investigate the diffusion dynamics of H atoms on the surface of stainless steel passivation films, this study employed the Forcite module within the Materials Studio software for simulation calculations.[21] Initially, a pristine 3 × 3 × 1 Fe_2O_3/Cr_2O_3 heterojunction structure was established. Subsequently, the Amorphous cell module was utilized to construct an amorphous unit of 10 H atoms. Fe_2O_3/Cr_2O_3 models with an Fe vacancy defect (V_{Fe}), an O vacancy defect (V_O), and a Cr vacancy defect (V_{Cr}) were created by sequentially removing one Fe atom as well as one O atom from Fe_2O_3 and one Cr atom from Cr_2O_3, respectively. Due to the formation energy of V_O defects in Fe_2O_3 is 9.56 eV,[22] while the formation energy of V_O defects in Cr_2O_3 is 5.12 eV,[23] indicating that V_O defects in Cr_2O_3 are more stable than Fe_2O_3. Therefore, there is only the V_O defect in the outer layer Fe_2O_3 in this study. H- Fe_2O_3/Cr_2O_3 models were built, and a 10 Å vacuum layer was inserted to isolate the surrounding lattice interactions. H-pristine, H−V_{Fe}, H−V_O, and H−V_{Cr} denote the models for the interaction of H with defect-free, containing V_{Fe}, V_O, and V_{Cr} defect passivation films, respectively, as shown in Figure 1.

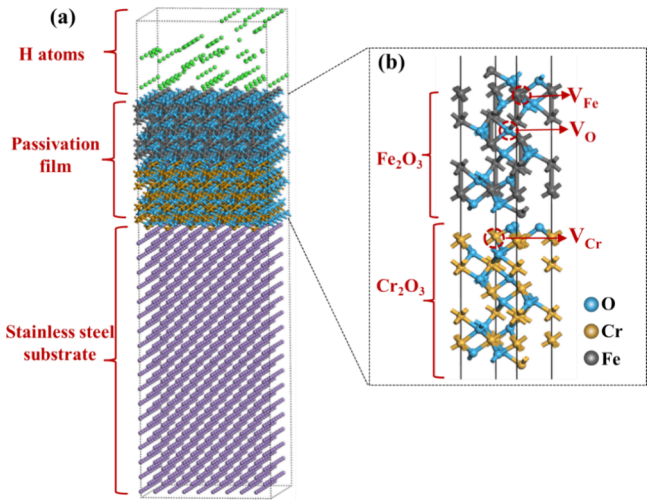

Figure 1. Passivation film model for stainless steel defects. (a) Passivation film model of hydrogen exposed stainless steel. (b) Enlarged image of the defect passivation film model.

The Forcite module was subsequently employed to optimize the structures of the four H−Fe_2O_3/Cr_2O_3 models. During structural relaxation, the energy convergence criterion was set to 1 × 10^{-5} kcal/mol, the force convergence criterion was 0.001 kcal/mol/Å, and the displacement convergence criterion was 1 × 10^{-5} Å. The COMPASS force field[24] was assigned for these calculations. Previous research has applied the COMPASS force field to the calculations of Fe_2O_3,[25] TiO_2,[26] MgO,[27] and CuO.[28] In order to substantiate the applicability of the COMPASS force field to study the properties of metal oxide structures, we have compared the experimental lattice parameters, *a* and *c*, and internal oxygen positional parameters, *u*, of the metal oxides (Fe_2O_3 and Cr_2O_3) with those of the minimized crystal structure predicted by the COMPASS force field. The lattice parameter values of $a = 5.035A^\circ$ and $c = 13.720A^\circ$ were used for the crystal structure of Fe_2O_3. By selecting the oxygen atom at position (*u*, *u*, 0), the coordinates of the oxygen atom were found to be (0.03333333, 0.36666667, 0.91666667). As for Cr_2O_3, the lattice parameters are *a* = 4.9589 Å and *c* = 13.59308 Å, and the coordinates of the oxygen atom were found to be (0.02733333, 0.36066667, 0.91666667). As the bonds between metal and oxygen atoms are ionic in nature, the parameters do not exist for covalent bonds between them, and hence, the bonds must be removed for optimization to proceed. After the optimization, for Fe_2O_3, the values of *a*, *c*, and (u_x, u_y, u_z) are 5.035 Å, 13.720 Å, and

https://doi.org/10.1021/acsomega.4c07162
ACS Omega 2024, 9, 46270−46275

Table 1. Total Energy (E_{Total})of the Stainless Steel Passivation Film System under Different Defect Types, Energy of the Single-Layer Oxide Film System ($E_{Fe_2O_3}$, $E_{Cr_2O_3}$), Hydrogen Atom Energy (E_H), and Interaction Energy between Passivation Film and Hydrogen ($E_{interaction}$)

	E_{Total}/eV	$E_{Fe_2O_3}$/eV	$E_{Cr_2O_3}$/eV	E_H/eV	$E_{interaction}$/eV
H-pristine	−53268.6571	−18240.05966	−35013.55444	−13.6028	−1.4402
H−V_{Fe}	−53267.9667	−18240.05966	−35013.55444	−13.6028	−0.7498
H−V_O	−53268.1948	−18240.05966	−35013.55444	−13.6028	−0.9779
H−V_{Cr}	−53267.41	−18240.05966	−35013.55444	−13.6028	−0.1931

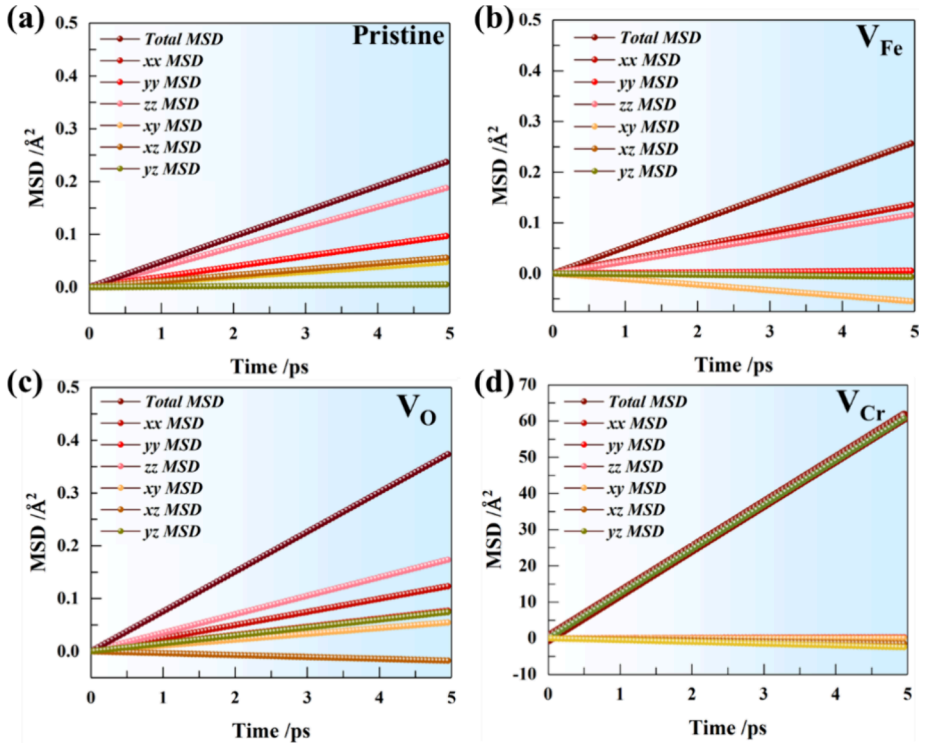

Figure 2. Root mean square displacement (MSD) of hydrogen atoms in passivation films with different defects over time: (a) pristine, (b) V_{Fe}, (c) V_O, and (d) V_{Cr}.

(0.03307476, 0.36382243, 0.90955606), respectively. For Cr_2O_3, the values of a, c, and (u_x, u_y, u_z) are 4.9589 Å, 13.59308 Å, and (0.02712130, 0.35786897, 0.90955606), respectively. The optimized geometric parameters are consistent with the experimental results.[29,30] After structural optimization, annealing was performed, in which the initial temperature was set to 300 K, dynamics steps per ramp was set to 5, and the total number of steps was 5000. Then, the isothermal isobaric ensemble (NPT) was used for dynamic simulation at 300 K, with a time step of 0.01 fs and a simulation duration of 5 ps.

3. RESULTS

3.1. Interaction Energy between Hydrogen Atoms and Fe_2O_3/Cr_2O_3 Passivation Films. The movement and diffusion of hydrogen within the passivation film inevitably interact with the film, and the strength of this interaction directly influences the hydrogen's diffusivity within the film. The interaction energy ($E_{interaction}$) between hydrogen and three types of defective passivation films is defined as follows[31]:

$$E_{interaction} = E_{H-Fe_2O_3/Cr_2O_3} - (E_{Fe_2O_3} + E_{Cr_2O_3} + E_H) \quad (1)$$

wherein, $E_{H-Fe_2O_3/Cr_2O_3}$ represents the total energy of the passivation film with hydrogen atoms. $E_{Fe_2O_3}$ and $E_{Cr_2O_3}$ represent the energies of the passivation films without H atoms, and E_H is the energy of one hydrogen atom. The calculation results are presented in Table 1. It is observed that the pristine passivation film exhibits the strongest interaction energy with hydrogen, at −1.4402 eV, indicating a substantial binding effect on hydrogen, thereby hindering further diffusion. In contrast, the interaction energies of V_{Fe} and V_O defective passivation films decrease by 0.9604 and 0.4623 eV, respectively, compared to the pristine film, suggesting a weakened binding effect for these two types of defects. Notably, the interaction energy between the V_{Cr} defective passivation film and hydrogen decreases by nearly an order of magnitude compared to the pristine film, indicating the weakest binding effect of V_{Cr} defects on hydrogen, thereby facilitating hydrogen's further diffusion within the film.

3.2. Diffusion Coefficient of the H Atom in Fe_2O_3/Cr_2O_3 Passivation Films. Furthermore, the diffusion behavior of hydrogen within the passivation film is investigated. The dynamics process of hydrogen diffusion is not only determined by hydrogen's inherent structure, charge distribution, and migration capability but also intimately

https://doi.org/10.1021/acsomega.4c07162
ACS Omega 2024, 9, 46270−46275

Table 2. Different Diffusion Coefficients of Hydrogen Atoms in Passivation Films[a]

	C_{xx}	C_{yy}	C_{zz}	C_{xy}	C_{xz}	C_{yz}	C_{Total}	ΔC_{Total}
pristine	1.368	0.055	1.167	0.552	0.068	0.066	3.275	
V_{Fe}	1.895	0.975	2.393	0.560	0.561	0.053	6.437	3.162
V_O	1.245	1.751	3.772	0.552	0.179	0.750	8.249	4.974
V_{Cr}	2.422	2.703	6.13	0.690	14.221	24.726	50.892	47.617

[a]The unit of diffusion coefficient is $10^{-10}m^2/s$.

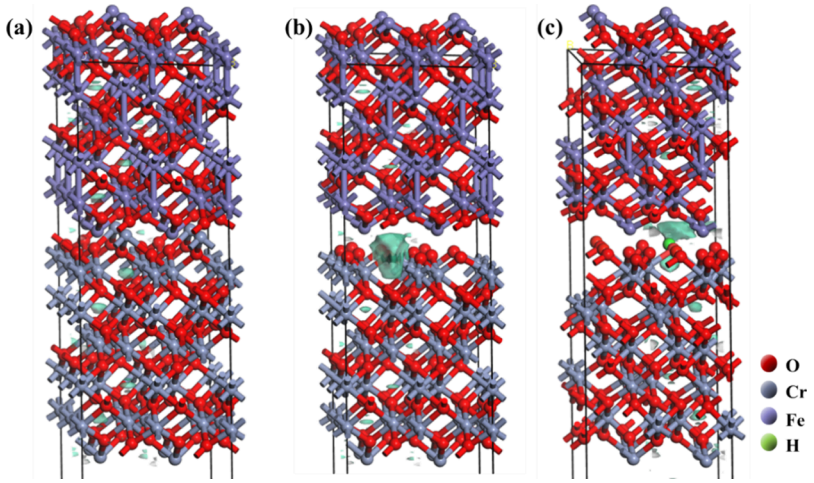

Figure 3. Charge density distribution results of Fe_2O_3/Cr_2O_3 passivation film. (a) Pristine passivation film without H atom, (b) V_{Cr} passivation film without H atom, and (c) V_{Cr} passivation film with H atom.

related to the interaction between hydrogen and the film as well as hydrogen's self-diffusion properties within the film. The self-diffusion performance of hydrogen atoms can be evaluated through mean squared displacement (MSD) and self-diffusion coefficient curves. Based on molecular dynamics simulations, the positions of hydrogen atoms over time are recorded and their displacements relative to their initial positions are calculated. The squared displacements are accumulated to obtain the total squared displacement, which is then divided by the number of hydrogen atoms to yield the average squared displacement, as shown in eq 2:

$$dD = \lim_{t\to\infty} \frac{1}{2Nt}\{|\vec{r_i}(t) - \vec{r_i}(0)|^2 \quad (2)$$

where $r_i \to (t)$ represents the displacement vector of the hydrogen atom at time t, $r_i \to (0)$ is the displacement vector of the hydrogen atom at time 0, N denotes the dimensionality of the system, which in this case is three for a three-dimensional system, and t represents time. By performing a linear fitting on the MSD−t curve, the diffusion coefficient d of the hydrogen atom can be obtained as one-sixth of the slope of the fitted linear function, as shown in Equation 3[32]:

$$\begin{aligned} d &= \frac{1}{6N_a}\lim_{t\to\infty}\frac{d}{dt}\sum_{i}^{N_a}\langle[r_i(t) - r_i(t_0)]^2\rangle \\ &= \frac{1}{6N_a}\lim_{t\to\infty}\frac{d}{dt}\sum_{i}^{N_a}\mathrm{MSD} \\ &= a/6 \end{aligned} \quad (3)$$

To analyze the hydrogen diffusion behavior along different directional paths within the passivation film, the motion of hydrogen atoms is decomposed to calculate the variations in the MSD across various path orientations. Consequently, the self-diffusion properties of hydrogen along the *xx, yy, zz, xy, xz,* and *yz* directional paths in passivation films with different defects are obtained, as depicted in Figure 2.

Furthermore, by solving the differential ratio of MSD with respect to diffusion time, the total diffusion coefficient of hydrogen in the four passivation film systems and also the diffusion coefficients along various path directions were obtained, as shown in Table 2. For pristine Fe_2O_3/Cr_2O_3, the diffusion coefficient of H atoms is $3.75 \times 10^{-10}m^2/s$, which is on the same order of magnitude as the previously studied diffusion coefficients of H atoms in Fe_2O_3 and Cr_2O_3.[32−34] For defective Fe_2O_3/Cr_2O_3, the diffusion coefficients (C_{xx}) of H atoms along the *xx, yy, zz, xy, xz,* and *yz* directions, the total diffusion coefficient (C_{Total}), and the difference between the diffusion coefficient of H atoms in the defect passivation film and their diffusion coefficient in the pristine passivation film (ΔC_{Total}) were obtained and shown in Table 2. It was found that the type of defect has little effect on the diffusion coefficient of H atoms along the *xx* and *xy* directions but has a significant effect on the diffusion coefficient of H atoms along the z direction, including *zz, xz,* and *yz* directions. Especially when H atoms diffuse along the *yz* direction, V_{Cr} defects cause an increase of 2 orders of magnitude in the diffusion coefficient of H atoms, which is consistent with the MSD results discussed earlier. In addition, when there are V_{Fe} or V_O defects in the outer layer of Fe_2O_3, compared to the original passivation film, the total diffusion coefficient of H atoms increases by 3.162×10^{-10} and $4.974 \times 10^{-10}m^2/s$, respectively. Once Cr vacancy defects appear in the inner layer of Cr_2O_3, the diffusion coefficient of H atoms will increase by 47.617×10^{-10} m^2/s, indicating that the diffusion of H atoms into the stainless steel matrix will be accelerated after defects appear in the inner layer of Cr_2O_3.

https://doi.org/10.1021/acsomega.4c07162
ACS Omega 2024, 9, 46270−46275

Based on the above analysis of diffusion coefficient, it was found that the diffusion coefficient of the passivation film containing V_{Cr} defects increased by 1 order of magnitude compared to other passivation film systems. Therefore, the properties, of V_{Cr} defects in Fe_2O_3/Cr_2O_3 were analyzed by calculating the electronic properties, and the results are shown in Figure 3. The charge density distribution of the defect-free passivation film is shown in Figure 3a, and the charge density distribution of the V_{Cr} defect passivation film before and after hydrogen atom diffusion is shown in Figure 3b,c, respectively. The light green color in the figure represents the charge density contour surface with a value of 0.03e/Å^3.

4. DISCUSSION

It is found that the total MSD slope is the highest for the V_{Cr} passivation film, indicating the strongest self-diffusion performance of hydrogen within this film. Additionally, based on the MSD results, hydrogen does not diffuse uniformly along all directional paths within the passivation film. For pristine V_{Fe} and V_O passivation films, hydrogen exhibits a preference for diffusion along the *zz*-directional path. Unlike defect-free and passivation films containing V_{Fe} and V_O defects, the diffusion anisotropy of hydrogen atoms in passivation films containing V_{Cr} defects is not significant, and H atoms tend to diffuse more concentrated along the *yz* direction. By comparing the vertical axis of MSD of four kinds of passivation films, it was found that the MSD of H atoms in the passivation film containing V_{Cr} defects increased by 2 orders of magnitude, indicating that under the same diffusion time, the diffusion rate of H atoms in the passivation film containing V_{Cr} defects is higher. For the V_{Fe} passivation film, the *zz* and *xx* paths serve as the primary channels for hydrogen diffusion. As for the V_O passivation film, the *yy* path is the second most significant diffusion channel after the *zz* path. On the other hand, for the V_{Cr} passivation film, hydrogen exhibits a preference for diffusion along the *yz* and *xz* paths. It was found that before the diffusion of H atoms, the charge density of the passivation film containing V_{Cr} defects was concentrated near the V_{Cr} defects compared to the defect-free Fe_2O_3/ Cr_2O_3. Once the H atoms diffused to the interface between Fe_2O_3 and Cr_2O_3, the charge density increased from the V_{Cr} defects to the vicinity of the H atoms.

5. CONCLUSIONS

In this study, the interaction energies between hydrogen and stainless steel passivation films with different defect structures have been calculated by molecular dynamics and the microscopic mechanisms of hydrogen diffusion by metal-atom vacancies and oxygen vacancy defect types have been revealed. By studying the self-diffusion properties of hydrogen in pristine films and three different defect-containing passivation films, the anisotropic diffusion behaviors and characteristics of hydrogen in passivation films with different defect structures are found, and it is found that Cr vacancy defects lead to an increase in the H diffusion coefficient by 1 order of magnitude. In addition, the main paths of hydrogen diffusion under different defect structures were predicted, which provided a theoretical basis for the prediction of hydrogen-induced cracking and the development of early warning technology for the surface failure of stainless steel.

AUTHOR INFORMATION

Corresponding Authors

Yuanshuang Liu − *State Key Laboratory of Chemical Safety, SINOPEC Research Institute of Safety Engineering Co. Ltd., Qingdao 266071, China*; orcid.org/0009-0008-9367-1503; Email: liuys.qday@sinopec.com

Feng Qiu − *State Key Laboratory of Chemical Safety, SINOPEC Research Institute of Safety Engineering Co. Ltd., Qingdao 266071, China*; Email: qiuf.qday@sinopec.com

Authors

Mindong Chen − *State Key Laboratory of Chemical Safety, SINOPEC Research Institute of Safety Engineering Co. Ltd., Qingdao 266071, China*

Dingrong Qu − *State Key Laboratory of Chemical Safety, SINOPEC Research Institute of Safety Engineering Co. Ltd., Qingdao 266071, China*

Haijun Hu − *School of Chemical Engineering and Technology, Xi'an Jiaotong University, Xi'an 710049, People's Republic of China*

Complete contact information is available at: https://pubs.acs.org/10.1021/acsomega.4c07162

Notes

The authors declare no competing financial interest.

ACKNOWLEDGMENTS

We are very grateful for the National Key Research andDevelopment Program of China (grant no. 2022YFC3004502) for the support of this research. We also would like to express our gratitude to the Excellent Youth Science and Technology Innovation Fund (grant no. YQ-90)of Sinopec Safety Engineering Research Institute Co., Ltd. and the National Natural Science Foundation of China (grant no.52405608 and no. 52201098) for their support of this research.

REFERENCES

(1) Wei, X. X.; Zhang, B.; Xu, Y. T.; Chen, Z. Y.; Li, X. L.; Ma, X. L. Transpassivation-Induced Structural Evolution of Oxide Film on 654SMO Super Austenitic Stainless Steel. *Corros. Sci.* **2024**, *232*, No. 112030.

(2) Hariharan, K.; Guo, X.; Huang, H. L.; Sridhar, N.; Srinivasan, J.; Hwang, J.; Frankel, G. S.; Schindelholz, E. J. Inter-Melt Pool Corrosion and Repassivation of SS316L Stainless Steel Processed by Laser Powder Bed Fusion. *Corros. Sci.* **2024**, *226*, No. 111668.

(3) Guo, L. Q.; Qin, S. X.; Yang, B. J.; Liang, D.; Qiao, L. J. Effect of Hydrogen on Semiconductive Properties of Passive Film on Ferrite and Austenite Phases in a Duplex Stainless Steel. *Sci. Rep.* **2017**, *7*, 3317.

(4) Mi, Z.; Chen, L.; Shi, C.; Gao, L.; Wang, D.; Li, X.; Liu, H.; Qiao, L. Prevent Hydrogen Damage in α-Cr_2O_3/α-Fe_2O_3 (0 0 0 1) Interface. *Appl. Surf. Sci.* **2019**, *475*, 294−301.

(5) Reddy, M. J.; Visibile, A.; Svensson, J. E.; Froitzheim, J. Investigation of coated FeCr steels for application as solid oxide fuel cell interconnects under dual-atmosphere conditions. *Int. J. Hydrogen Energy* **2023**, *48* (38), 14406−14417.

(6) Malladi, S. B. A.; Tam, P. L.; Cao, Y.; Guo, S.; Nyborg, L. Corrosion Behaviour of Additively Manufactured 316L and CoCrNi. *Surf. Interface Anal.* **2023**, *55* (6−7), 404−410.

(7) Paswan, S.; Meena, L. K.; Guguloth, K.; Shariff, S. M.; Singh, R. Oxidation and Hot Corrosion Studies of Laser Hybrid Welded IN617 and P91 Alloys. *T INDIAN I METALS* **2024**, *77* (5), 1275−1286.

(8) Li, Q.; Mo, L. B.; Wang, J.; Yan, K.; Tang, T.; Rao, Y. C.; Yao, W. Q.; Cao, J. L. Performances of Cr_2O_3−Hydrogen Isotopes

Permeation Barriers. *Int. J. Hydrogen Energy* **2015**, *40* (19), 6459−6464.
(9) Liao, L.; Cheng, Y.; Zhang, H.; Yuan, X.; Li, F. Comparing Electrochemical Passivation and Surface Film Chemistry of 654SMO Stainless Steel and C276 Alloy in Simulated Flue Gas Desulfurization Condensates. *Materials* **2024**, *17* (8), 1827.
(10) Yue, X.; Du, H.; Hou, L.; Wang, Q.; Liu, X.; Wei, H.; Wei, Y. Study on Corrosion Resistance Mechanisms of Gradient-Structured Austenitic Stainless Steel Materials Based on Passivation Behavior. *Mater. Lett.* **2023**, *341*, No. 134265.
(11) Xie, D.-G.; Wang, Z.-J.; Sun, J.; Li, J.; Ma, E.; Shan, Z.-W. In Situ Study of the Initiation of Hydrogen Bubbles at the Aluminium Metal/Oxide Interface. *Nat. Mater.* **2015**, *14* (9), 899−903.
(12) Macdonald, D. D. The History of the Point Defect Model for the Passive State: A Brief Review of Film Growth Aspects. *Electrochim. Acta* **2011**, *56* (4), 1761−1772.
(13) Choudhary, S.; Thomas, S.; Birbilis, N. Evolution of Passivity and Passivity-Breakdown for Cr and Cr-Containing Alloys. In *244th ECS Meeting*; IOP Publishing Ltd: 2023, MA2023−02, 1082.
(14) Inman, S. B.; Han, J.; Wischhusen, M. A.; Qi, J.; Agnew, S. R.; Ogle, K.; Scully, J. R. Passivation and Localized Corrosion Resistance of $Al_{0.3}Cr_{0.5}Fe_2Mo_xNi_{1.5}Ti_{0.3}$ Compositionally Complex Alloys: Effect of Mo Content. *Corros. Sci.* **2024**, *227*, No. 111692.
(15) Wang, F.; Zou, D. N.; Yan, X. Y.; Zhang, Y. B.; Pan, J. X.; Cheng, Y. X.; Xu, R.; Jiang, Y. C. Phase Precipitation and Corrosion Properties of Copper-Bearing Ferritic Stainless Steels by Annealing Process. *J. Iron. Steel Res. Int.* **2023**, *30* (11), 2280−2292.
(16) Shao, Z.; Yu, D.; Shao, D.; Du, Y. F.; Zheng, D.; Qiu, Z.; Wu, B. A Protective Role of Cl^- Ion in Corrosion of Stainless Steel. *Corros. Sci.* **2024**, *226*, No. 111631.
(17) Zeng, Y. M.; Luo, J. L.; Norton, P. R. New Interpretation of the Effect of Hydrogen on the Ion Distributions and Structure of Passive Films on Microalloyed Steel. *J. Electrochem. Soc.* **2004**, *151* (6), B291.
(18) Zhang, K.; Wu, L.; Zhou, Z.; Zhang, X.; Wang, G.; Yang, G. Effects of Hydrogen on Passivation and Semiconductive Properties of Passive Film on Fe-based Amorphous Coatings. *Appl. Surf. Sci.* **2023**, *635*, No. 157754.
(19) Qin, M.; Hu, Q.; Cheng, Y. F. Passivation of X80 Pipeline Steel in a Carbonate/Bicarbonate Solution and the Effect of Oxide Film on Hydrogen Atom Permeation into the Steel. *Int. J. Hydrogen Energy* **2024**, *70*, 1−9.
(20) Ma, J.; Luo, H.; Hu, X.; Pan, Z.; Li, X. Electrochemical Study on the Effect of Hydrogen on the Passive Film of Selective Laser Melted 316L Stainless Steel in a Proton Exchange Membrane Water Electrolyzer Environment. *Int. J. Hydrogen Energy* **2023**, *48* (51), 19396−19410.
(21) Wang, J.; Wei, Z.; Liu, Y.; Jing, X.; Liu, F.; Cao, H.; Tan, Q.; Zhao, W. Preparation and Molecular Simulation of an Environmentally Friendly Dust-Fixing Agent based on Chitosan-Gelatin. *Environ. Sci. Pollut. Res.* **2023**, *30* (42), 95312−95325.
(22) Guan, Y.; Zhang, G.; Wang, R.; Wang, Y.; Liu, Y. Study on the Synergistic Effect and Oxygen Vacancy of CeO_2/Fe_2O_3 Oxygen Carrier for Improving Reactivity in Carbon Monoxide Chemical Looping Combustion. *Fuel* **2024**, *357*, No. 129832.
(23) Lebreau, F.; Islam, M. M.; Diawara, B.; Marcus, P. Structural, Magnetic, Electronic, Defect, and Diffusion Properties of Cr_2O_3: A DFT+U Study. *J. Phys. Chem. C* **2014**, *118* (31), 18133−18145.
(24) Costa, S. N.; Almeida-Neto, F. W. Q.; Campos, O. S.; Fonseca, T. S.; De Mattos, M. C.; Freire, V. N.; Homem-de-Mello, P.; Marinho, E. S.; Monteiro, N. K. V.; Correia, A. N.; De Lima-Neto, P. Carbon Steel Corrosion Inhibition in Acid Medium by Imidazole-Based Molecules: Experimental and Molecular Modelling Approaches. *J. Mol. Liq.* **2021**, *326*, No. 115330.
(25) Ta, T. D.; Tieu, A. K.; Zhu, H.; Kosasih, B. Adsorption of Normal-Alkanes on Fe(110), FeO(110), and Fe_2O_3(0001): Influence of Iron Oxide Surfaces. *J. Phys. Chem. C* **2015**, *119* (23), 12999−13010.
(26) Prathab, B.; Subramanian, V.; Aminabhavi, T. M. Molecular Dynamics Simulations to Investigate Polymer−Polymer and Polymer−Metal Oxide Interactions. *Polymer* **2007**, *48* (1), 409−416.
(27) Zhao, L.; Liu, L.; Sun, H. Semi-ionic Model for Metal Oxides and Their Interfaces with Organic Molecules. *J. Phys. Chem. C* **2007**, *111* (28), 10610−10617.
(28) Loya, A.; Stair, J. L.; Uddin, F.; Ren, G. Molecular Dynamics Simulation on Surface Modification of Quantum Scaled CuO Nano-Clusters to Support Their Experimental Studies. *Sci. Rep.* **2022**, *12* (1), 16657.
(29) Naveas, N.; Pulido, R.; Marini, C.; Hernández-Montelongo, J.; Silván, M. M. First-Principles Calculations of Hematite (α-Fe_2O_3) by Self-Consistent DFT+U+V. *iScience* **2023**, *26* (2), No. 106033.
(30) Abdullah, M. M.; Rajab, F. M.; Al-Abbas, S. M. Structural and Optical Characterization of Cr_2O_3 Nanostructures: Evaluation of its Dielectric Properties. *AIP Adv.* **2014**, *4* (2), No. 027121.
(31) Traidia, A.; Chatzidouros, E.; Jouiad, M. Review of Hydrogen-Assisted Cracking Models for Application to Service Lifetime Prediction and Challenges in the Oil and Gas Industry. *Corros. Rev.* **2018**, *36* (4), 323.
(32) Xing, B.; Wu, J.; Cheng, J.; Zhang, L.; Wu, M. Hydrogen Diffusion in α-Fe_2O_3: Implication for an Effective Hydrogen Diffusion Barrier. *Int. J. Hydrogen Energy* **2020**, *45* (56), 32648−32653.
(33) Chen, C.; Yu, H.; Zheng, S. First-Principles Study of Hydrogen Diffusion Mechanism in Cr_2O_3. *Sci. China Technol. Sci.* **2011**, *54* (1), 88−94.
(34) Li, Q.; Mo, L.-B.; Wang, J.; Yan, K.; Tang, T.; Rao, Y.-C.; Yao, W.-Q.; Cao, J.-L. Performances of Cr_2O_3−Hydrogen Isotopes Permeation Barriers. *Int. J. Hydrogen Energy* **2015**, *40* (19), 6459−6464.

https://doi.org/10.1021/acsomega.4c07162
ACS Omega 2024, 9, 46270−46275